J. Fluid Mech. (2010), *vol.* 663, *pp.* 253–267. © Cambridge University Press 2010
doi:10.1017/S0022112010003502

Tuning turbines in a tidal channel

ROSS VENNELL†

Ocean Physics Group, Department of Marine Science, University of Otago, Dunedin 9054, New Zealand

(Received 23 February 2010; revised 21 June 2010; accepted 28 June 2010;
first published online 12 October 2010)

As tidal turbine farms grow they interact with the larger scale flow along a channel by increasing the channel's drag coefficient. This interaction limits a channel's potential to produce power. A 1D model for a tidal channel is combined with a theory for turbines in a channel to show that the tuning of the flow through the turbines and the density of turbines in a channel's cross-section also interact with the larger scale flow, via the drag coefficient, to determine the power available for production. To maximise turbine efficiency, i.e. the power available per turbine, farms must occupy the largest fraction of a channel's cross-section permitted by navigational and environmental constraints. Maximising of power available with these necessarily densely packed farms requires turbines to be tuned for a particular channel and turbine density. The optimal through-flow tuning fraction varies from near 1/3 for small farms occupying a small fraction of the cross-section, to near 1 for large farms occupying most of the cross-section. Consequently, tunings are higher than the optimal through-flow tuning of 1/3 for an isolated turbine from the classic turbine theory. Large optimally tuned farms can realise most of a channel's potential. Optimal tunings are dependent on the number of turbines per row, the number of rows, as well as the channel geometry, the background bottom friction coefficient and the tidal forcing.

Key words: coastal engineering, shallow water flows

1. Introduction

Many possible sites for generating electricity from tidal currents are found in the high flows through narrow channels and straits that connect parts of the ocean with different tidal regimes. It is essential to have a method to assess the potential of a tidal channel to generate power. Early assessment methods were based on the average kinetic energy (KE) flux through the undisturbed channel (see review by Blunden & Bahaj 2007). Garrett & Cummins (2005) (hereafter GC05) showed that KE flux considerably overestimates a channel's potential because it does not account for the influence the turbines have on the flow. Their simple one-dimensional model showed how extracting power from turbines increases a channel's total drag coefficient, slowing flow along the channel. This interaction of turbines with the flow results in a peak in the power curve, which quantifies a channel's potential to produce power. This paper takes GC05's result to the next level. Whereas they showed how the interaction between the turbines and the macroscopic flow along the channel limits its potential, this work explores how the aspects of the internal configuration of a farm, turbine through-flow tuning and density interact with the larger scale flow

† Email address for correspondence: ross.vennell@otago.ac.nz

https://doi.org/10.1017/S0022112010003502 Published online by Cambridge University Press

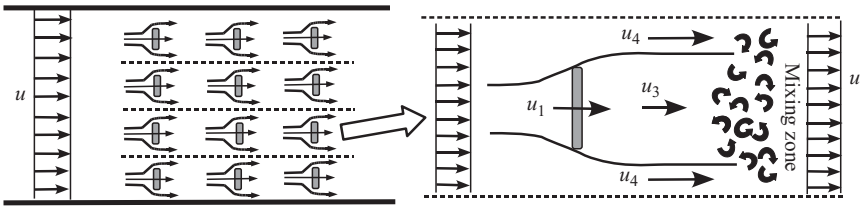


FIGURE 1. A schematic of a turbine farm in a channel with gaps between turbines arranged in rows to form a grid. Adjacent turbines create virtual walls, given by the dashed lines. These walls enhance the flow bypassing the turbines relative to the slower flows through the turbines; so that $u_4 \geqslant u > u_1 > u_3$. Adapted from Garrett & Cummins (2007).

and how these aspects determine the maximum power available for production. The work aims to improve understanding of how to scale up single turbines into large tidal energy farms. It may be the first to show that maximising production requires turbines to be tuned for a particular tidal channel.

GC05's estimate of potential assumes that turbines occupy the entire cross-section of a channel. However, to allow for navigation of vessels and marine life along a channel, farms will require gaps between turbines. When there are gaps, Garrett & Cummins (2007) (hereafter GC07) showed that mixing of the enhanced flow through the gaps downstream of the turbines with the slower flow passing through the turbines dissipates energy (figure 1). As a result of this wake dissipation, there is a distinction between a channel's potential, which is the maximum power lost by the flow due to the turbines, and the smaller power available for electricity production.

The GC07 model maximises the power available by tuning the velocity downstream of the turbine, u_3, to be 1/3 of the free-stream flow u (figure 1). This through-flow tuning would typically be done by adjusting the pitch of the turbine's blades. GC07's optimal tuning for a channel did not vary with the fraction of a channel's cross-section taken up by the turbines and was the same as that found by Lanchester (1915) and Betz (1920) for an isolated turbine. In GC07, the farm's drag coefficient is dependent on how the turbines are tuned. GC07's optimal tuning of 1/3 is based on the assumption that the free-stream flow is constant, i.e. there is no interaction between the drag coefficient associated with power extraction and the free-stream flow. However, in GC05's model, flow along the channel is not constant, as there is an interaction between power extraction and the free-stream flow along the channel, via the farm's gross drag coefficient. Consequently, the optimally tuned turbines of GC07 cannot be directly combined with the GC05 model (as done briefly in GC07 and Garrett & Cummins 2008 to comment on the desirable number of turbine rows) because the free-stream flow u is a function of the tuning.

GC07 gives the optimal tuning for a given along-channel flow, whereas the properly combined GC05 and GC07 model developed here gives the optimal tuning for a given headloss between the ends of a tidal channel. This properly combined model may be the first to span the transition from a single isolated turbine generating power from the flow's kinetic energy (the classic Lanchester–Betz turbine) to large farms occupying the whole cross-section generating power from headloss across the farm (GC05). Spanning this transition is made possible by the novel realisation that optimal tunings vary in tidal channels.

This paper uses a deliberately simple idealised model to explore optimal tunings, i.e. the internal configuration of the farm required to maximse power production. The understanding provided by the simplified 1D model used here is critical to those

https://doi.org/10.1017/S0022112010003502 Published online by Cambridge University Press

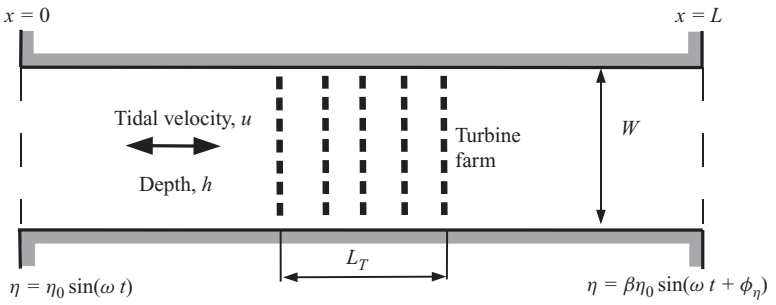


FIGURE 2. Schematic diagram of a turbine farm with a grid of turbines in a narrow channel which connects two large water bodies. Channel has length L, depth h and width W. L_T is the length of channel occupied by the turbine farm. Flow is forced by differences in water level, η, between the ends.

developing 2D and 3D numerical models of the sites of proposed turbine farms and will enable them to more efficiently explore how to optimize their farms.

2. Channel model

GC05's model for turbines in a tidal channel connecting two large water bodies is outlined. Here, for simplicity, only channels with a uniform rectangular cross-section are considered and the effects of a variable cross-section and an exiting jet included in GC05's model will be discussed in a future work. Consider a shallow narrow tidal channel with a uniform rectangular cross-section that connects two large water bodies (figure 2). The channel has a turbine farm confined to a short section of the channel, with turbines arranged in a grid. Tidal currents are driven through the channel by the difference in surface elevation between the water bodies and are assumed uniform across the channel. In addition, it is assumed that the channel is short enough that velocity does not vary along the channel. Vennell (1998) derived conditions for channels with a range of dynamical balances to be considered short enough to neglect the variation in the transport along a channel. Here the starting point is the 1D shallow water momentum balance for the channel as a whole

$$\rho A_c L \frac{\partial u}{\partial t} = -\rho g A_c(\eta|_{x=L} - \eta|_{x=0}) - \rho C_D W L|u|u - \rho C_T A_c|u|u, \tag{2.1}$$

where $u(t)$ is the along channel velocity, η is the displacement of the water's free surface (assumed small compared to the water depth h), A_c is the channel's cross-sectional area, L is the channel's length and W is its width. The first term in (2.1) is the rate of change of momentum of the fluid within the channel, the second is the pressure force due to the water level difference between the ends of the channel, the third is the force due to background bottom friction and the last is the force due to the turbines. C_D is the drag coefficient for bottom friction and C_T the farm's gross drag coefficient based on the cross-sectional area. For a single forcing frequency, ω, the water level difference between the ends can be written in the form $\Delta\eta_0 \sin(\omega t + \phi_g)$, where $\Delta = \sqrt{1 - 2\beta\cos\phi_\eta + \beta^2}$ and $\phi_g = \tan^{-1}(\beta \sin\phi_\eta/(1 - \beta\cos\phi_\eta))$. Here β is the ratio of the amplitudes of the surface elevation at the ends and ϕ_η is the phase lead of the tidal elevation at $x = L$ (figure 2). Also, ϕ_g is the phase of the water level difference between the ends of the channel relative to the surface elevation's phase at

https://doi.org/10.1017/S0022112010003502 Published online by Cambridge University Press

$x = 0$. With this the governing equation (2.1) becomes

$$\frac{\partial u}{\partial t} = a\sin(\omega t + \phi_g) - \left(\frac{C_D}{h} + \frac{C_T}{L}\right)|u|u, \tag{2.2}$$

where $a = g\eta_0\Delta/L$. After non-dimensionalising the velocity by a/ω, the amplitude of the velocity in the channel with no background friction or turbines, and time by $1/\omega$ the governing equation becomes as given in GC05:

$$\frac{\partial u'}{\partial t'} = \sin(t' + \phi_g) - (\lambda_0 + \lambda_T)\,|u'|u'. \tag{2.3}$$

The non-dimensional drag coefficients are $\lambda_0 = \alpha C_D L/h$ and $\lambda_T = \alpha C_T$, where $\alpha = a/\omega^2 L$. The parameter α is introduced for conciseness, it has no obvious physical meaning, but in combination with the farm's drag coefficient αC_T, i.e. λ_T, gives the relative importance of drag on the farm and the tidal forcing. Similarly, the parameter $\alpha C_D L/h$, i.e. λ_0, gives the relative importance of background bottom friction and the tidal forcing. In λ_0 the geometric ratio L/h occurs because the bottom friction drag coefficient is based on the channel's horizontal area, whereas the farm's drag coefficient is based on the channel's cross-sectional area.

Non-dimensionally the power lost by the flow due to the turbines averaged over a tidal cycle relative to a channel's potential can be expressed as

$$\frac{\overline{P}_{lost}}{\overline{P}_{max}} = \frac{\lambda_T\ \overline{|u'(t', \lambda_0 + \lambda_T)|^3}}{\lambda_{T\,peak}\,\overline{|u'(t', \lambda_0 + \lambda_{T\,peak})|^3}}, \tag{2.4}$$

where the overbar indicates an average over a tidal cycle. $\overline{P}_{max}$ is the maximum power that can be extracted, i.e. the channel's potential, given by the average power lost by flow at the peak in the power curve (figure 3*a*, discussed below). $\lambda_{T\,peak}$ is the farm's gross drag coefficient at the peak in the power lost curve. It will be shown later that $\lambda_{T\,peak}$ (3.1) depends only on λ_0. Thus for any given channel the non-dimensional power lost curve (2.4) is solely dependent on the farm's gross drag coefficient, λ_T.

The nonlinear equation (2.3) was solved numerically using Runge–Kutta 45 integration using the approximate analytical velocity solution in the Appendix (see (A 3)) as an initial condition. The model was run until it achieved a steady state. The average power and other information were then calculated from the last full tidal cycle.

2.1. *Turbine farm with gaps*

Gaps between turbines will likely be necessary to allow the passage of vessels and marine life along a channel (figure 1). GC07 modelled the power produced by turbines in a channel where some flow is allowed to bypass the turbines through gaps. Their model had uniform water depth, uniform steady flow upstream and downstream of the turbines and ignored bottom friction. Their results are expressed in terms of the fraction of the cross-sectional area taken up by the turbines, ϵ, and thus, as they note, can be applied either to a single turbine or to many turbines within the same cross-section occupying a total fraction ϵ. Here ϵ is effectively the cross-sectional turbine density. They also noted that a farm may consist of multiple rows of turbines and it is assumed that the spacing between rows is large enough to allow the high flow bypassing the turbines in one row to fully mix with the retarded flow passing through the same turbines before encountering the next row.

GC07 showed that the force on the turbines is related to the various velocities in figure 1. The force can be expressed as $F = \rho N_R C_{T1} A_c u^2$, where C_{T1} is the drag

https://doi.org/10.1017/S0022112010003502 Published online by Cambridge University Press

coefficient for a single row of turbines based on the channel's cross-sectional area and N_R is the number of rows of turbines in the farm. The total number of turbines in the farm can be written $N = N_R \epsilon A_c / A_T$, where A_T is the blade area of one turbine. From GC07's (2.8) the drag coefficient for one row of untuned turbines can be written as

$$C_{T1} = \frac{\epsilon}{2}\left(r_4^2 - r_3^2\right), \tag{2.5}$$

where $r_i = u_i/u$ is the ratio of the various velocities near the turbine to the free-stream flow. By using Bernoulli and balancing mass and momentum within control volumes GC07 found an expression for the flow through the gaps between the turbines, u_4 (GC07, equation (2.23)), which can be rewritten as

$$r_4 = \frac{1 - r_3 + \sqrt{\epsilon - 2\epsilon\, r_3 + (1 - \epsilon + \epsilon^2) r_3^2}}{1 - \epsilon}. \tag{2.6}$$

In addition, the velocity passing through the turbines relative to the free stream can be expressed in terms of r_3 and r_4 (GC07, equation (2.9)) as

$$r_1 = \frac{r_3(r_4 + r_3)}{r_4 + 2r_3 - 1}. \tag{2.7}$$

GC07 also showed that the power lost by the flow due to the turbines and power available are

$$P_{lost} = Fu = \rho N_R C_{T1} A_c u^3, \tag{2.8}$$

$$P_{avail} = Fu_1 = \rho N_R C_{T1} A_c u^3 r_1. \tag{2.9}$$

The difference between P_{lost} and P_{avail} is the energy dissipated as the fast bypassing flow mixes with the slower flow passing through the turbines, with r_1 being the fraction of power lost available for production (GC07). Equations (2.5) and (2.6) show C_{T1} depends only on ϵ and r_3, and from (2.6) and (2.7). r_1 also depends only on ϵ and r_3. The powers (2.8) and (2.9) are thus functionally expressed as $P_{lost}(N_R, u, \epsilon, r_3)$ and $P_{avail}(N_R, u, \epsilon, r_3)$. Turbine pitch can be adjusted to give particular through-flows measured by r_3. Thus r_3 can be used as a turbine tuning parameter. For an isolated turbine with a constant free-stream flow, u, Lanchester–Betz found the optimal tuning of $r_3 = 1/3$. GC07 found the same optimal tuning, $r_3 = 1/3$ for a turbine in a channel. However, in a tidal channel driven by a head loss between the ends, the free-stream along-channel flow is not constant but depends on the farm's gross drag coefficient, i.e. $u(t', \lambda_0 + \lambda_T)$, where

$$\lambda_T = N_R^* C_{T1}(\epsilon, r_3) \tag{2.10}$$

and the non-dimensional number of rows $N_R^* = \alpha N_R$. The dependence of the velocity u on r_3, via the drag coefficient λ_T, means the tuning required to maximize both the power lost and available in a tidal channel differs from that given by GC07.

2.2. *Combined model*

Here the GC07 model, which has steady flow and ignores bottom friction, is combined with the tidal channel model of GCO5, which includes bottom friction. As they note in Garrett & Cummins (2008) the differing assumptions may place limits on the applicability of the combined model. Here the combination is rationalised by assuming that the farm takes up only a short section of the channel, $L_T \ll L$. Consequently, the force of the turbines dominates bottom friction and flow inertia within a short farm and the headloss across the farm is in a quasi-steady state balance with the

https://doi.org/10.1017/S0022112010003502 Published online by Cambridge University Press

velocity. In the broader extent of the channel bottom friction and inertia may still be significant.

To solve the combined model specified values of ϵ, r_3 and N_R^* are used to calculate λ_T. With λ_0 the channel model (2.3) is solved numerically to find the average power lost and available in a single tidal cycle. Peaks in the power lost and available curves were found using numerical searches based on golden section search and parabolic interpolation.

The use of r_3 as the turbine tuning parameter of the combined model warrants some comment. Tuning blade pitch to obtain an optimal flow fraction downstream of the turbine, r_3, is reasonable for an isolated turbine. However, in the confined channel of GC07 and here, the wake size downstream of the turbine depends on the turbine spacing, thus the through-flow fraction at the turbine, r_1, may be a better tuning parameter. The choice of r_3 as the tuning parameter was made firstly for easy comparison with the classic and GC07 optimal tunings. Secondly, substituting for r_4, (2.6), in (2.7) and rearranging would give a complicated expression for r_3 as a function of r_1 and ϵ. Thus r_3 was chosen as the tuning parameter partly for mathematical convenience.

The model and its results are presented in terms of a non-dimensional or re-scaled number of rows $N_R^* = \alpha N_R$. If this had not been done it would be necessary to explore the effects of the non-dimensional parameter $\alpha = a/\omega^2 L$. Thus 'non-dimensionalising' the number of rows reduces the number of cases and plots which must be presented. However, the number of rows is an integer and thus for any specific channel N_R^* is not a continuous variable but takes on discrete values which are integer multiples of α. If turbines of the same blade area are installed then ϵ also only takes on discrete values which are integer multiples of A_T/A_c as turbines are added to a cross-section.

For a fixed tuning r_4 and C_{T1} become large as $\epsilon \to 1$. As a result with sufficient rows, λ_T (see (2.10)) can be made to exceed $\lambda_{T\,peak}$ and push the farm beyond the peak in the power curve. Thus for any tuning ϵ and N_R^* can be varied to give a range of farm drag coefficients.

Free-surface effects restrict GC07's model to small Froude numbers, $u/\sqrt{gh} \ll 1$. As they note, the enhanced flow though the gaps further restricts the model's applicability as $\epsilon \to 1$ because r_4 becomes large. Thus the combined model requires $r_4 a U_0/\omega\sqrt{gh} \ll 1$, where $U_0(\lambda_0 + \lambda_T)$ is from (A 3). This condition varies with turbine tuning and density, as well as the channel's geometry and tidal forcing. However, the need for navigation will generally restrict ϵ to be sufficiently small that this Froude number condition is easily meet.

3. Power curves and similarity

Figure 3 gives examples of power curves for a channel. The curves of power lost due to the turbines in figure 3(*a*) exhibits GC05's peak at the farm's optimal drag coefficient, $\lambda_{T\,peak}$ corresponding to the channel's potential, $\overline{P}_{max}$. A channel's potential decreases as the importance of bottom friction, λ_0, increases because bottom friction dissipates energy, which is then not available for power production. Useful results from the approximate analytic solution to GC05's channel model given in the Appendix are that

$$\lambda_{T\,peak} \approx \frac{3\pi\sqrt{2}}{8} + 2\lambda_0, s \tag{3.1}$$

and that the amplitude of the along channel velocity (see (A 3)) decreases monotonically with increasing farm drag coefficient. A consequence of these results

https://doi.org/10.1017/S0022112010003502 Published online by Cambridge University Press

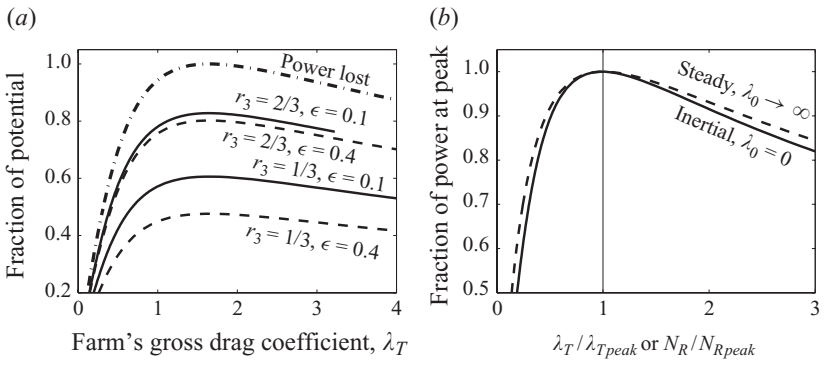


FIGURE 3. (*a*) Curves of power relative to the channel's potential for a channel with no bottom friction, $\lambda_0 = 0$. Chained dashed line is the power lost by the flow due to the turbines. Other curves are power available for generation for different values of r_3 and ϵ. Solid lines are for $\epsilon = 0.1$ and dashed are for $\epsilon = 0.4$. (*b*) Power curves of power lost or power available normalized by $\lambda_{T\,peak}$ and the power at their respective peaks for constant values of r_3 and ϵ. Solid line is the inertial limit, $\lambda_0 = 0$, and dashed line the steady limit, $\lambda_0 \to \infty$.

is that increasing the importance of bottom friction, λ_0, both reduces a channel's potential and shifts the peak in the power curve to higher λ_T (see (3.1)). Effectively, this implies that as bottom friction becomes more important more turbines are required to realise less power when r_3 and ϵ are constant.

Scaling the power lost (2.4) by the peak power lost and the farm drag coefficient by the location of the peak gives normalised power curves

$$\frac{\overline{P}_{lost}}{\overline{P}_{max}} = S\frac{\overline{|u'(t', S + S_0)|^3}}{\overline{|u'(t', 1 + S_0)|^3}}, \tag{3.2}$$

where $S = \lambda_T/\lambda_{T\,peak}$ and $S_0 = \lambda_0/\lambda_{T\,peak}$. These normalised power curves are thus identical for any given λ_0, i.e. they exhibit similarity. In addition, plotting normalised power curves (see figure 3*b*) shows there is little variation between the two extreme dynamical balances of the channel, the inertial limit, $\lambda_0 = 0$, and the quasi-steady limit, $\lambda_0 \to \infty$. This demonstrates that the normalised power lost curves exhibit near self-similarity across the full range of dynamical balances, which simplifies the presentation of some later results.

3.1. *Effects of tuning*

The fraction of a channel's potential available varies with r_3 and ϵ in figure 3(*a*). At $\epsilon = 0.1$ increasing r_3 from 1/3 to 2/3 substantially increases the power available, demonstrating that optimal tunings for the tidal channel can differ from GC07's value of 1/3. In figure 3(*a*) increasing ϵ decreases the power available, as in GC07. However, figure 4 (discussed later) demonstrates that whether ϵ decreases or increases the power available at a given tuning, r_3, depends on whether ϵ is less than or greater than an optimal ϵ value.

Non-dimensionally the power lost curve depends only on λ_T and λ_0. Also the location of its peak, $\lambda_{T\,peak}$, is independent of the internal configuration of the turbine farm, but depends only on one channel parameter, λ_0 (3.1). Power lost (2.8) and power available (2.9) are both proportional to the force on the turbines. Hence functionally, for constant r_3 and ϵ, the power available has the same dependence on λ_T as the

https://doi.org/10.1017/S0022112010003502 Published online by Cambridge University Press

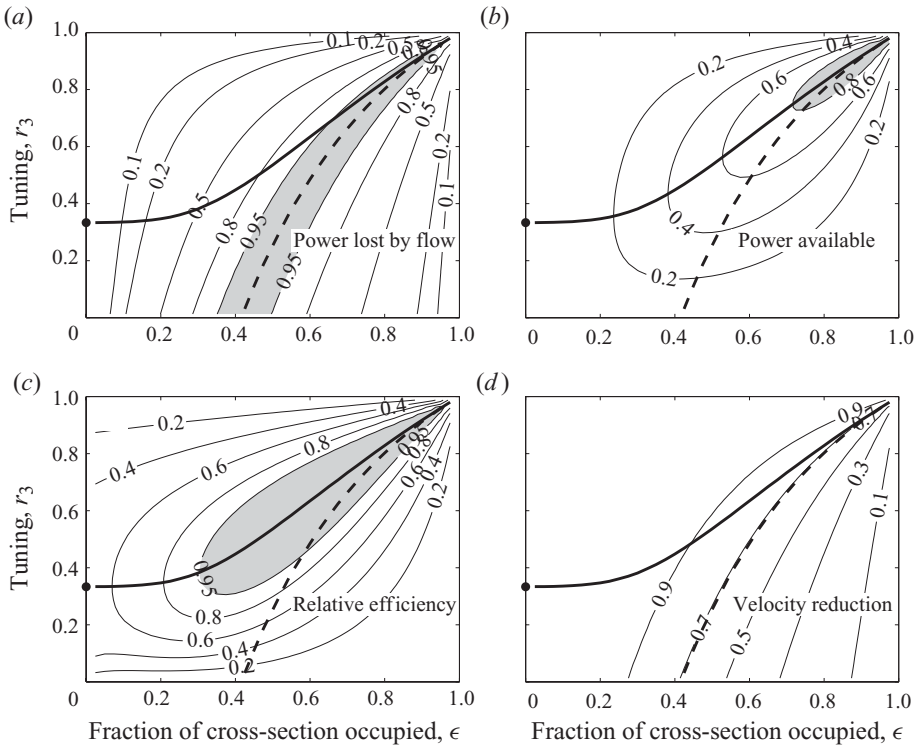


FIGURE 4. Power contours for an inertial channel, $\lambda_0 = 0$, for $N_R^* = 1$. (*a*) Power lost by flow relative to a channel's potential, $\overline{P}_{lost}/\overline{P}_{max}$. (*b*) Fraction of a channel's potential available for production, $\overline{P}_{avail}/\overline{P}_{max}$. (*c*) The relative efficiency of the turbines (4.1). (*d*) The reduction in velocity relative to the undisturbed channel. In all plots the thick dashed curve is the tuning, $r_{3\,peak}$, which maximises power lost, $\overline{P}_{lost}$, and the thick solid curve the tuning, $r_{3\,opt}$, which maximises power available, $\overline{P}_{avail}$. The shaded areas indicate regions with high values.

power lost, the only difference is that power available is reduced by a factor of $r_1(r_3, \epsilon)$. Consequently, the peaks in the power available curves for constant r_3 and ϵ also occur at $\lambda_{T\,peak}$, as demonstrated in figure 3(*a*). In addition, the power available curves when normalised by $\lambda_{T\,peak}$ and the power at their respective peaks will also be given by those in figure 3(*b*). Thus power available also exhibits near self-similarity across the dynamical range when r_3 and ϵ are constant. This is a consequence of λ_T being proportional to N_R^* (2.10), so that $\lambda_T/\lambda_{T\,peak} = N_R^*/N_{R\,peak}^* = N_R/N_{R\,peak}$ for constant r_3 and ϵ, where $N_{R\,peak}^* = \lambda_{T\,peak}/C_{T1}$.

4. Optimal turbine tunings

4.1. *Fixed number of rows, N_R^**

Figure 4 shows how tuning and power vary with ϵ for a fixed number of turbine rows, $N_R^* = 1$. Figure 4(*a*) contours the fraction of a channel's potential lost by the flow. The dashed line, $r_{3\,peak}$, corresponds to the tuning required at the peak in the power curves in figure 3(*a*). All points on this curve have that same power lost and the same gross drag coefficient, $\lambda_{T\,peak}$. The curve simply gives different combinations of ϵ and r_3 which give the same farm drag coefficient (see (2.10)).

https://doi.org/10.1017/S0022112010003502 Published online by Cambridge University Press

There are two optimal tuning curves in figure 4. The first $r_{3\,peak}$ (thick dashed curve) maxmises the power lost by the flow. The second $r_{3\,opt}$ (thick solid curve) maximises the power available, which is given in figure 4(b). These two optimal tuning curves differ, particularly, for small ϵ. Comparing the two curves in figure 4(b), increasing r_3 to move from the dashed curve, $r_{3\,peak}$, around a contour to the solid curve, $r_{3\,opt}$, yields the same power from a smaller ϵ, i.e. fewer turbines. The power available at this optimal tuning is maximised at high ϵ for $r_{3\,opt} \to 1$. That is, the turbines occupy almost the entire cross-section and there is no flow reduction downstream of the turbines, as in GC05. At small ϵ the optimum tuning tends towards $r_{3\,opt} = 1/3$, the tuning of Lanchester–Betz's isolated turbine. Figure 4(b) shows that by adjusting the tuning it is possible to achieve a smooth transition from maximising the power available from an isolated turbine, to almost realising a channel's potential at high ϵ.

A measure of the effectiveness or efficiency of each turbine is the power available per turbine normalised by the channel's potential, $\overline{P}_{avail}/N\overline{P}_{max}$. Here the relative efficiency will be used, which can be expressed as

$$RE = \frac{\overline{P}_{avail}}{N\overline{P}_{max}}\alpha\frac{A_c}{A_T} = \frac{\overline{P}_{avail}}{\epsilon N_R^*\overline{P}_{max}}. \tag{4.1}$$

Figure 4(c) gives the relative efficiency for $N_R^* = 1$. While the values on the contours of this figure do not have a particular meaning, their relative values show highest efficiencies when optimally tuned to $r_{3\,opt}$. Maximum efficiency requires ϵ to be large, i.e. turbines to occupy as much of the cross-section as possible. Interestingly, for this example, when $\epsilon > 0.3$ the output per turbine is almost constant. Thus the power available for optimally tuned turbines grows almost linearly with ϵ and the number of turbines in the cross-section.

As noted combinations on the dashed line, $r_{3\,peak}$, in figure 4 have the same farm drag coefficient, and hence the same velocity, given in figure 4(d). On the solid $r_{3\,opt}$ curve the drag coefficient varies, thus for a given ϵ tuning using $r_{3\,opt}$ yields more power from stronger along-channel flows than using $r_{3\,peak}$. Consequently, a secondary advantage of tuning using $r_{3\,opt}$ is less disturbance of the channel's environment by a given number of turbines in the cross-section.

4.2. *Fixed cross-sectional density, ϵ*

Figure 5(a) contours the fraction of a channel's potential available for power production from turbines occupying 25 % of the cross-section. Again power lost is maximised on the thick dashed line, $r_{3\,peak}$ and power available is maximised along the thick solid line, $r_{3\,opt}$. The same power available on the dashed line can be obtained by moving around a contour in figure 5(b) to the solid line. Thus the same yield from a farm tuned to $r_{3\,peak}$ is available from a farm with fewer rows tuned to the higher $r_{3\,opt}$. Viewed from a turbine efficiency perspective, figure 5(c), efficiency is maximised by a single row of optimally tuned turbines for which $N_R^* = \alpha$.

For large optimally tuned farms available power is maximised on the $r_{3\,opt}$ curve on the upper right of the figure, demonstrating that even when occupying less than the entire cross-section, it is almost possible to achieve a channel's potential when there are gaps, though this requires a very large number of turbines, i.e. $N_R, N \to \infty$.

Note that as $\lambda_T \propto N_R$ at constant r_3 and ϵ (see (2.10)), the power curves obtained from horizontal slices of both figures 5(a) and 5(b) are self-similar and look like the curves in figure 3(b). In addition the near-similarity across the full dynamical range means that the power available contours for an inertial channel in figure 5(d) plotted with a normalised x-axis will be very similar to the contours for a steady

https://doi.org/10.1017/S0022112010003502 Published online by Cambridge University Press

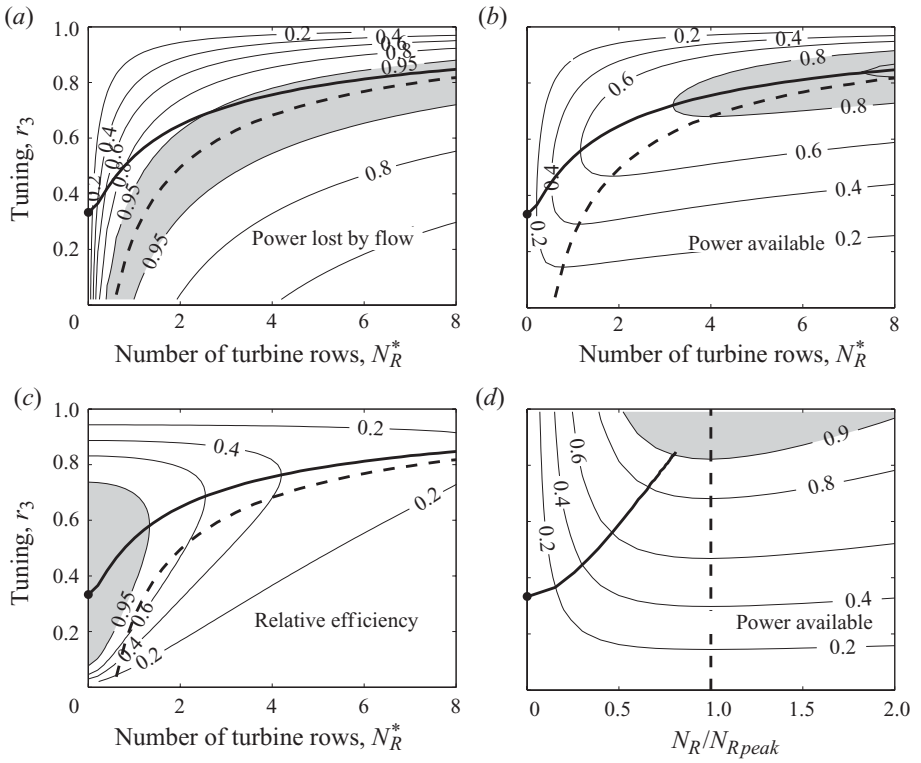


FIGURE 5. Dependence of averaged power or tidal velocity on the number of rows and turbine tuning for an inertial channel, $\lambda_0 = 0$, with $\epsilon = 0.25$. (*a*) Power lost by flow due to the turbines relative to a channel's potential, $\overline{P}_{lost}/\overline{P}_{max}$. (*b*) Fraction of a channel's potential available for production, $\overline{P}_{avail}/\overline{P}_{max}$. (*c*) The relative efficiency of the turbines (see (4.1)). (*d*) Fraction of power available with x-axis normalised by the number of rows at peak power lost, $N_{R\,peak}$. The thick dashed line is $r_{3\,peak}$ and thick solid line is $r_{3\,opt}$. Solid dot is $r_3 = 1/3$. Shaded regions indicate highest values.

state channel, $\lambda_0 \to \infty$. The number of rows required for this normalisation, i.e. the number required to maximise power lost to the turbines, can be obtained from the approximate analytic solution (see (3.1)) giving an expression for the dashed curve in figure 5 as

$$N^*_{R\,peak} = \frac{1}{C_{T1}(r_3, \epsilon)} \left(\frac{3\pi\sqrt{2}}{8} + 2\lambda_0 \right). \tag{4.2}$$

Again the number of rows is an integer, thus for a specific channel this expression must take discrete values which are multiples of α.

4.3. *At optimal tuning,* $r_{3\,opt}(N_R^*, \epsilon)$

Figure 6(*a*) shows how optimal tuning $r_{3\,opt}$ varies with N_R^* and ϵ, from 1/3 in the lower left for small farms which occupy only a small fraction of the channel cross-section, to near 1 in the upper right for large farms occupying most of the cross-section. The power available in figure 6(*b*) can approach the channel's potential, $\overline{P}_{max}$, for large farms occupying most of the cross-section. The main implication of figure 6(*b*) is that adding turbines to an optimally tuned farm will always increase the farm's total output, provided ϵ remains the same or increases. Also horizontal sections of figure 6(*b*) demonstrate a 'law of diminishing returns', as the gain per

https://doi.org/10.1017/S0022112010003502 Published online by Cambridge University Press

	A – Shallow channel	B – Tidal strait
Depth, h	20 m	100 m
Length, L	2 km	50 km
Width, W	500 m	10 km
Surface phase diff./Press. grad. phase, ϕ_η /ϕ_g	10°/275°	180°/0°
Tidal amplitude, η_0/Headloss amplitude, $\Delta\eta_0$	1.0 m/0.17 m	0.7 m/1.4 m
Undisturbed current amplitude	2.7 m s^{-1}	1.9 m s^{-1}
α/λ_0	22/5.4	0.3/0.35
Peak power lost, $\overline{P}_{max}$	9.0 MW	5.5 GW
One row – power available, $\overline{P}_{avail}$	4.8 MW	0.4 GW
Current amplitude	2.0 m s^{-1}	1.8 m s^{-1}
$r_1/r_{3\,opt}/r_4$	0.72/0.52/1.2	0.55/0.34/1.4
Ten rows – power available, $\overline{P}_{avail}$	8.2 MW	2.3 GW
Current amplitude	1.6 m s^{-1}	1.6 m s^{-1}
$r_1/r_{3\,opt}/r_4$	0.93/0.86/1.1	0.66/0.46/1.3

TABLE 1. Two hypothetical examples of high flow tidal channels with optimally tuned turbines. Both have semidiurnal tides, $\epsilon = 0.25$, $\beta = 1$, and $C_D = 0.0025$. For each example N_R^* is α times the number of rows.

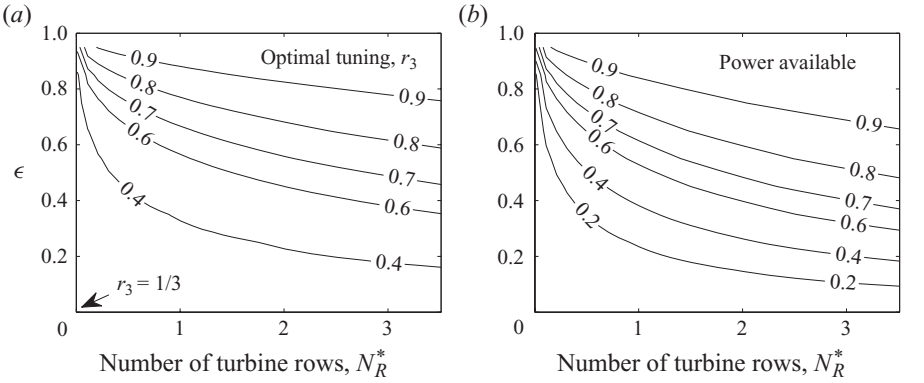


FIGURE 6. Tuning and power at optimal tuning for an inertial channel, $\lambda_0 = 0$. (a) Optimal tuning, $r_{3\,opt}(\epsilon, N_R^*)$. ($b$) Fraction of a channel's potential available for production, $\overline{P}_{avail}/\overline{P}_{max}$.

turbine row reduces as an optimally tuned farm grows. Further, horizontal sections show that for a given ϵ the extra return on each additional turbine is largest at high ϵ. As a result, to minimise the number of turbines it is essential to occupy as much of the channel's cross-section as possible. The relative efficiency (4.1) (not shown) emphasises this, by demonstrating that the highest return per optimally tuned turbine is at high ϵ and small N_R^*, consistent with figures 4(c) and 5(c).

It should be emphasized that for a specific channel and turbine not all combinations of ϵ and N_R^* in figure 6 are possible because the number of rows and the number of turbines in a row are integers. This may require a compromise between the number of turbines in each row and the number of rows to achieve near optimal power availability.

To give some context to the results table 1 gives two hypothetical examples of high flow channels with optimally tuned turbines taking up 25 % of the channels' cross-sections. The first, a shallow 20 m deep entrance to a large embayment, lies near the steady state limit $\lambda_0 = 5.4$. The shallow channel has a potential of $\overline{P}_{max} = 9.0$ MW

https://doi.org/10.1017/S0022112010003502 Published online by Cambridge University Press

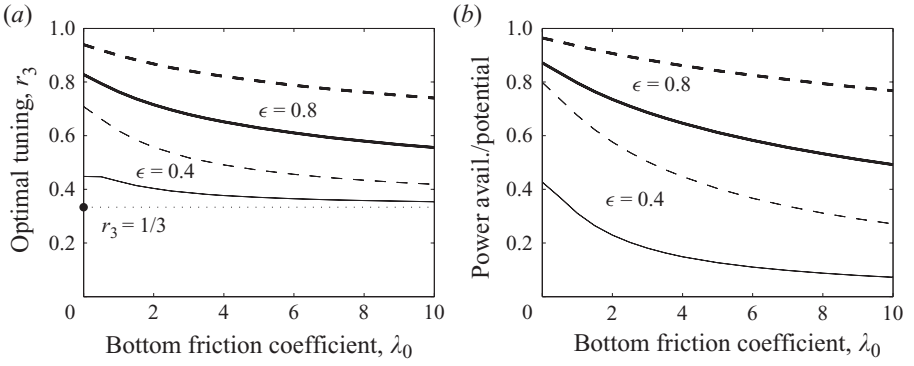


FIGURE 7. Effect of dynamical balance, λ_0, on (a) optimal tuning and (b) fraction of potential available for power production, $\overline{P}_{avail}/\overline{P}_{max}$. Thin lines are for $\epsilon = 0.4$ and thick lines for $\epsilon = 0.8$. Solid lines are for $N_R^* = 1$ and dashed lines are for $N_R^* = 5$. Inertial channels are on the left and quasi-steady state channels are towards the right.

with 4.8 MW of this available from a single row of turbines tuned to $r_{3\,opt} = 0.52$ and 8.2 MW available from ten rows tuned to $r_{3\,opt} = 0.86$ (though ten rows would probably violate the model assumption of widely spaced rows confined to a short section of the shallow channel). The second channel, a 100 m deep tidal strait connecting two water bodies with semi-diurnal tides in anti-phase, lies near the inertial limit, $\lambda_0 = 0.3$. The strait's potential is huge, $\overline{P}_{max} = 5.5$ GW, but only 0.4 GW is available from a single row and 2.3 GW from ten rows, both at much lower tunings than the shallow channel. In both examples, the farm's electricity output will be significantly less than the power available due to the electro-mechanical efficiency of the turbines and drag on the turbines' support structures.

4.4. *Effects of dynamical balance*

Figure 7(a) illustrates the effect dynamical balance has on optimal tuning. This figure shows that, not only as noted earlier does $r_3 \to 1/3$ for small ϵ and N_R, but r_3 also tends towards 1/3 for steady state channels, $\lambda_0 \to \infty$.

Figure 7(b) shows that, in all cases, as the effects of bottom friction become more important, $\lambda_0 \to \infty$, the fraction of a channel's potential that is available for power production decreases. So not only does increasing importance of bottom friction reduce a channel's potential and require more turbines to achieve that potential, but bottom friction also reduces the fraction of the potential available for power production. Thus the energy available per square kilometre in deep inertia dominated tidal straits will be relatively much higher than in shallow tidal channels.

Increasing the number of rows in figure 7 increases both optimal tunings and the fraction of power available. To realise a large fraction of a channel's potential requires ϵ to be large. However if navigation or environmental constraints allow only a small ϵ, then a large number of turbine rows are required to achieve a large fraction of potential. Together figures 7(a) and 7(b) demonstrate that in either case, large ϵ or large N_R^*, optimal tunings are well above the 1/3 of an isolated turbine across a realistic dynamical range for high flow tidal channels of $\lambda_0 = 0.35$ to 5.4 given by the examples in table 1.

https://doi.org/10.1017/S0022112010003502 Published online by Cambridge University Press

5. Discussion

A tidal channel's potential depends on properties of the channel, such as $\lambda_{T\,peak}$ (see (3.1)), and is independent of the farm's internal configuration, i.e. N_R^*, ϵ and r_3. For a given along-channel flow, GC07 found that the useful fraction of the potential, the fraction available, was $2/3(1+\epsilon)$. Superficially, their result, that power available decreases as ϵ increases, would suggest that farms in tidal channels need to occupy as small a fraction of the channel's cross-section as possible and at most 2/3 of a channel's potential is available for electricity production. However, for a given headloss the results presented here show that it is possible to realise most of a channel's potential if economics permits installation of sufficient optimally tuned turbines. Also, to minimise the required number of turbines, i.e. maximise turbine efficiency, the farm must be configured to occupy the largest fraction of a channel's cross-section permitted by the navigational and environmental constraints. Furthermore, for optimally tuned farms, the fluid dynamics yields no optimum number of turbines in figure 6(*b*), but efficient optimally tuned farms should grow by densely filling rows first, then adding rows up to the maximum that the economics of the diminishing return on new turbines will allow. The most significant result is that densely packed turbines will need to be tuned for a particular channel and turbine density to maximise a farm's output. Of the two optimal tuning curves $r_{3\,peak}$ and $r_{3\,opt}$, the latter can deliver the same power from fewer turbines with less disturbance to along-channel flows.

Tunings which maximise power available vary from near $r_{3\,opt}=1/3$, for small farms occupying only a small fraction of the cross-section, to near $r_{3\,opt}=1$, for large farms occupying most of the cross-section. Between these two extremes the source of the tidal energy changes smoothly from the flow's kinetic energy, Lanchester–Betz, to headloss across the farm (GC05). Figure 6(*a*) gives the optimal tuning, $r_{3\,opt}$, for farms made up of a grid of turbines, with a non-dimensionalised number of turbines per row, ϵ, and a non-dimensionalised number of rows N_R^*. The figure shows optimal tuning is strongly affected by how turbines are arranged as a grid, as is power available. The tuning is also specific to a particular channel as it varies with its non-dimensional drag coefficient $\lambda_0=\alpha C_D L/h$ and $N_R^*=\alpha N_R$. As a result, optimal tunings for a particular channel are influenced by its dimensional drag coefficient, length, width, depth, tidal frequency and the amplitude of the tidal forcing.

The model presented is very simple so its ability to predict precise tunings for real farms is limited; however, it demonstrates the necessity of tuning turbines for a particular channel, which has significant implications. One is that there is a strong incentive to construct turbines with the ability to tune blade pitch in real time throughout a tidal cycle in order to maintain the r_3 ratio which maximises their output. However, the maintenance costs of difficult-to-access turbines will encourage the use of mechanically simpler fixed pitched turbines, though this will reduce average turbine output. Fixed tunings will probably be set before turbine installation to achieve the maximum average output for the farm when fully developed. How to optimise fixed tunings will be the subject of a future work. However, the fixed tuning will probably be significantly greater than the $r_3=1/3$ of an isolated turbine and thus fixed pitch turbines will perform suboptimally until a farm is fully developed.

In the simple geometry of the model flow is assumed uniform across the channel outside of the farm. However, as $\lambda_0 \propto 1/h$, the variation of water depth across a channel will result in variation of the dynamical balance (e.g. Vennell 2006), which in turn will require tunings to vary across the channel (figure 6*a*). Consequently, turbines will need to be individually tuned when water depth varies significantly across a channel. This will also be addressed in a future work.

https://doi.org/10.1017/S0022112010003502 Published online by Cambridge University Press

Turbine flow interaction means that developers using 2D and 3D numerical models to estimate the power available from a proposed turbine farm site will need to include idealised turbines in their models. The necessity of tuning these turbines within efficient densely packed farms for a specific channel and turbine density will require multiple model runs. As a result estimating the power available for a particular site using 2D and 3D numerical models will be an iterative and computationally expensive process.

Appendix. Approximate analytic solution

Despite a quadratic drag law there is an approximate analytic solution to GC05's model equation (2.3). LeProvost (1991) showed that for a single frequency sinusoidal current, $u' = U_0 \sin(t' + \phi_g - \phi_u)$, the drag term $|u'|u'$ in (2.3) can be expanded to

$$|u'|u' = \frac{8}{3\pi} U_0 u' + U_0^2 \sum_{n=1,2,\ldots} \frac{8(-1)^{n+1}}{(2n-1)(2n+1)(2n+3)\pi} \sin((2n+1)t' + \phi_g - \phi_u). \quad \text{(A 1)}$$

The terms in the summation are less than 4 % of the size of the first term and $|u'|u'$ is well approximated by the first term alone and with (2.2) becoming

$$U_0 \cos(t' + \phi_g - \phi_u) + \hat{\lambda}\, U_0{}^2 \sin(t' + \phi_g - \phi_u) \approx \sin(t' + \phi_g), \quad \text{(A 2)}$$

where $\hat{\lambda} = (8/3\pi)(\lambda_0 + \lambda_T)$. Karsten *et al.* (2008) obtained and solved by an integration technique a similar equation for turbines in a channel connected to a lagoon. The velocity amplitude and phase can be found by expanding (A 2) to give two equations which have solutions

$$U_0 = \frac{\left(\sqrt{4\hat{\lambda}^2 + 1} - 1\right)^{1/2}}{\sqrt{2}\,\hat{\lambda}} \quad \text{(A 3)}$$

and $\phi_u = \tan^{-1} 1/U_0\hat{\lambda}$. The analytic power curves (not shown) are very similar to the numerical solution in figure 3, with the analytical solution slightly overestimating the power lost, particularly in inertial channels. Differentiating the analytic power lost gives an expression for the peak's location, $\lambda_{T\,peak}$, which is too long to be useful, though there are simple exact peak locations for both the dynamical extremes. Fortuitously, a figure in Karsten *et al.* (2008) demonstrates that $\lambda_{T\,peak}$ is approximately linear between the two dynamical extremes, so that

$$\lambda_{T\,peak} \approx \frac{3\pi\sqrt{2}}{8} + 2\lambda_0 \quad \text{(A 4)}$$

which, considering it is the approximate location of the peak in an approximate solution, agrees well with the numerical peak in figure 3(*a*).

REFERENCES

Betz, A. 1920 Das Maximum der theoretisch möglichen Ausnutzung des Windes durch Windmotoren. *Gesamte Turbinenwesen* **26**, 307–309.

Blunden, L. S. & Bahaj, A. S. 2007 Tidal energy resource assessment for tidal stream generators. *Proc. Inst. Mech. Eng. Part* A: *J. Power Energy* **221**, 137–146(10).

Garrett, C. & Cummins, P. 2005 The power potential of tidal currents in channels. *Proc. R. Soc.* A **461**, 2563–2572.

Garrett, C. & Cummins, P. 2007 The efficiency of a turbine in a tidal channel. *J. Fluid Mech.* **588**, 243–251.

https://doi.org/10.1017/S0022112010003502 Published online by Cambridge University Press

Garrett, C. & Cummins, P. 2008 Limits to tidal current power. *Renew. Energy* **33**, 2485–2490.

Karsten, R. H., McMillan, J. M., Lickley, M. J. & Haynes, R. D. 2008 Assessment of tidal current energy in the Minas Passage, Bay of Fundy. *Proc. Inst. Mech. Engrs* A: *J. Power Energy* **222** (5), 493–507.

Lanchester, F. W. 1915 A contribution to the theory of propulsion and the screw propeller. *Trans. Inst. Naval Archit.* **LVII**, 98–116.

Le Provost, C. 1991 Generation of overtides and compound tides. In *Tidal Hydrodynamics* (ed. B. Parker), pp. 269–296. Wiley.

Vennell, R. 1998 Oscillating barotropic currents along short channels. *J. Phys. Oceanogr.* **28** (8), 1561–1569.

Vennell, R. 2006 ADCP measurements of momentum balance and dynamic topography in a constricted tidal channel. *J. Phys. Oceanogr.* **36** (2), 177–188.

https://doi.org/10.1017/S0022112010003502 Published online by Cambridge University Press